Lung Cancer 127 (2019) 112–121

Contents lists available at ScienceDirect

Lung Cancer

journal homepage: www.elsevier.com/locate/lungcan

Promising preclinical platform for evaluation of immuno-oncology drugs using Hu-PBL-NSG lung cancer models

Kyoung Ho Pyo[a,b,1], Jae Hwan Kim[b,1], Ji-Min Lee[c,1], Sung Eun Kim[b], Jae Seok Cho[b], Sun Min Lim[d,*], Byoung Chul Cho[b,**]

[a] Severance Biomedical Science Institute, Yonsei University College of Medicine, Seoul, South Korea
[b] Division of Medical Oncology, Department of Internal Medicine, Yonsei Cancer Center, Yonsei University College of Medicine, Seoul, South Korea
[c] Brain Korea 21 PLUS Project for Medical Science, Yonsei University, South Korea
[d] Department of Internal Medicine, Division of Medical Oncology, CHA Bundang Medical Center, Seongnam-si, Gyeonggi-do, South Korea

ARTICLE INFO

Keywords:
Humanized mouse
Hu-PBL-NSG
Immunotherapy
EML4-ALK

ABSTRACT

Background: With the advance of immunotherapy, treatment of non-small-cell lung cancer (NSCLC) has revolutionized by having anti-PD-1 therapy in front-line setting. In this era of cancer immunotherapy, humanized mouse models which recapitulate human immune system, are needed for predicting immunotherapy response in patients. We established a Hu-PBL-NSG mouse model which can be used as a preclinical testing platform for assessing efficacy of different immunotherapeutic agents.

Materials and methods: Hu-PBL-NSG mouse model was established by engrafting human peripheral blood mononuclear cells (PBMCs) into NOD/scid/IL-2Rγ$^{-/-}$ (NSG) mice. Cytokine array was performed to assess serological similarity between patient and the Hu-PBL-NSG mouse, and microscopic immune cell infiltration was observed in various organs mouse model. Human anti-PD-1 therapy was treated for assessing drug efficacy in patient-derived tumor.

Results: hCD3$^+$hCD45$^+$ T-cells and antigen presenting cells (dendritic cells, macrophages, and MDSC) increased in the serum of Hu-PBL-NSG mouse 24 h after the transfusion of human PBMCs, and CD3 + T cells were observed in lung, liver, kidney, spleen sections. Cytokine arrays of human and Hu-PBL-NSG mouse revealed high similarity of Th1, Th2, Th17-related cytokines. A tumor xenograft was engrafted from an *EML4-ALK* patient, and Hu-PBL-NSG mouse was sacrificed for histological analyses. hCD3$^+$ T cells were infiltrated within the tumor, and CD11c + cells, which represent antigen-presenting capability, were seen in spleen, lung, liver and kidney. When anti-PD-1 Ab was treated intraperitoneally, xenograft tumor showed significant reduction in volume after day 6, and increased expression of immune response-related genes on microarray analysis in the tumor. Mostly IFN-gamma and its related gene sets were significantly changed (FDR < 0.25, GSEA).

Conclusion: Hu-PBL-NSG mouse model which highly resembles human immune system was successfully established. This model could be a strong preclinical model for testing efficacy of immunotherapeutic agents, and also for pursuing novel immunotherapy treatment strategies in advanced NSCLC.

1. Introduction

Recent development of checkpoint inhibitors has shed light on non-small-cell lung cancer (NSCLC) patients without targetable alterations. The excitement about using immunotherapy to treat NSCLC has been driven by results from clinical studies evaluating antibodies to programmed death receptor 1 (PD-1) and programmed death ligand 1 (PD-L1) [1]. A strategy targeting immune checkpoints such as PD-1/PD-L1 showed promising clinical benefits and introduced a paradigm shift in treatment by showing significantly improved progression-free survival

Abbreviations: NSCLC, non-small-cell lung cancer; PBMC, peripheral blood mononuclear cell; NSG, NOD/*scid*/IL-2Rγ$^{-/-}$; GVHD, graft versus host disease; NOG, NOD/Shi-*scid*-IL2rγ^{null}

* Corresponding author at: CHA Bundang Medical Center, Division of Medical Oncology, 59 Yatap-ro, Seongnam-si, Gyeonggi-do, South Korea.
** Corresponding author at: Yonsei Cancer Center, Division of Medical Oncology, Yonsei University College of Medicine, 50 Yonsei-ro, Seodaemun-Gu, Seoul, South Korea.
E-mail addresses: smlim@cha.ac.kr (S.M. Lim), cbc1971@yuhs.ac (B.C. Cho).
[1] These authors contributed equally as first authors.

https://doi.org/10.1016/j.lungcan.2018.11.035
Received 12 September 2018; Received in revised form 23 November 2018; Accepted 26 November 2018

and overall survival compared to conventional platinum-based chemotherapy in NSCLC [2,3]. Although PD-L1 expression by immunohistochemistry was used for selecting patients amenable for anti-PD1 therapy, PD-L1 overexpression cannot simply be a biomarker to tailor the treatment of immune checkpoint inhibitors due to the complexity of tumor immunity [4]. In addition, various immune checkpoint inhibitors are currently in development and are in needs translation into the clinic [5]. In this aspect, a robust animal model for assessing efficacy of immuno-oncology drugs should be developed. “Mouse avatars” which entail implantation of patient tumor samples in mice for drug efficacy studies should be developed to identify a personalized therapeutic regimen.

Immunodeficient mice engrafted with human cells and tissues have provided an exciting alternative to *in vitro* studies with human tissues and nonhuman primates for the study of human immunobiology [6,7]. The humanized mouse model should meet the following criteria. First, it has a patient-derived xenograft tumor which is used for testing drug efficacy. Second, it has hemato-lymphoid organs and immune cells that act in response to immunotherapy. Third, it should not have allograft rejection. So far, a number of human-mouse chimeric models with human immune cells have been developed [6,8]. The simplest approach to engraft a human immune system is to inject human peripheral blood mononuclear cells (PBMCs) into adult immunodeficient mice, and this is termed the Hu-PBL-SCID model [7,9]. This model allows rapid expansion of activated T cells after one week, but is limited by a lethal xenogeneic graft-*versus*-host disease (GVHD) within a few weeks, which limits experimental period. Hu-PBL-NOD-*scid* IL2rγ^{null} (NSG) model enables a complete immune system including both innate and adaptive immune cells. This model is advantageous in that it has reduced development of xenogeneic GVHD [10]. For Hu-PBL-NSG model, three types of avatars can be established: 1) human avatar consisting of tissue and PBMC from the same patient, 2) allogeneic avatar consisting of tissue from the patient and PBMC from a HLA-class 1 matched donor, 3) allogeneic cell line model consisting of human cancer cell line and PBMC from a HLA-class 1 matched donor. Human avatar model requires perfectly matched HLA type, in which each patient has their own tumor growing in an *in vivo* system. Allogeneic avatar and allogenic cell line models utilize PBMCs from a donor which makes the PBMC source simple.

In this study, we successfully developed Hu-PBL-NSG mice for testing efficacy of immuno-oncology drugs. These mice enable investigation of immunological phenomena and tumor response to immune-oncology drugs which can be applied to future clinical management of the patient’s tumor.

2. Materials & methods

2.1. Human cell line for tumor engraftment

H3122 cells were kindly provided by Dr Okamato at Kyushu University (Fukuoka, Japan). Cells were cultured in RPMI 1640 medium (HyClone) supplemented with 10% heat-inactivated fetal bovine serum (FBS) at 37 °C in 5% CO_2. Hu-PBL-NSG mice were injected 1.0×10^6 cells of H3122 cell lines in subcutaneous under anesthesia.

2.2. Experimental animals

All experimental animals were followed with the ethical standards of the Institutional Animal Care and Use Committee of Avison Bio Medical Research Center in Yonsei University (IACUC ID: 2016-0002). Female NOD/scid/IL-2R$\gamma^{-/-}$ mice (NOD.cg-Prkdc^{scid}Il2rg^{tm1Wjl}/SzJ abbreviated to NSG) and female hu-CD34-NSG mice were obtained from The Jackson Laboratory and were used between 6–8 weeks of age. The mice were maintained under pathogen-free conditions according to SPF guideline (room temperature, 40–60% humidity).

2.3. Preparation of PBMC

Fresh whole blood from patients was collected with EDTA tube (ethylenediamine tetraacetic acid tube, BD Vacutainer). On average, 1.0×10^7 cells were isolated from 5 ml of whole blood (Supplementary Fig. 1A). The collected whole blood was 2x diluted with Hanks' Balanced Salt solution (HBSS, Gibco, Rockville, MD, USA) for loading on Ficoll-paque (Pharmacia, Uppsala, Sweden) (Supplementary Fig. 1B). The blood-loaded sample on Ficoll solution is centrifuged at 2000 rpm for 20 min (Acceleration /Break = lowest / zero), and middle layer was collected as PBMC (Supplementary Fig. 1C). The collected cells were enumerated and stored in liquid nitrogen tank until us (Supplementary Fig. 1D). All study participants provided informed consent, and was approved by the institutional review board of Severance Hospital.

2.4. PBMC injection process for Hu-PBL-NSG mouse model

The PBMC from healthy/lung cancer patients was stored in liquid nitrogen tank until use. The restored PBMC is washed one time with HBSS (Gibco), and finally mixed with 200 µl of HBSS (Gibco) for intravenous injection in the tail of recipient mouse (NSG mouse). The equipment for tail vein injection is shown in Supplementary Fig. 2 Fig. 2A–B. Injection of 1.0×10^7 PBMCs in the lateral side of tail vein was performed (Supplementary Fig. 2C-D).

2.5. Immunotherapy and measurement of tumor size

Anti-PD-1(clone RMP1-14, BioXCell, NY, USA) was administered at 200 µg (i.p.) per mouse, twice a week. Tumor dimensions were measured three times with a digital caliper and tumor volume was calculated by the following formula: tumor volume = [length × width^2]/2.

2.6. Flow cytometry

Mouse blood was collected from facial vein with EDTA tube (BD). Other organs were collected and digested for single cells. RBCs were removed using RBC lysis buffer (Biolegend, San Diego, CA, USA) and then cells were washed by PBS (Dulbecco's phosphate-buffered saline, Corning Cellgro ®, Corning, NY, USA.) Cells were blocked with human anti-CD16/32 (Human TruStain FcX, Biolegend, San Diego, CA, USA) for 10 min at 4 °C. Afterwards cells were stained with human anti-CD3 (PE-Cy7, Biolegend, San Diego, CA, USA), human anti-CD45 (APC, Biolegend, San Diego, CA, USA), human anti-CD34 (PE, Biolegend. San Diego, CA, USA), human anti-CD11b (PE-Cy5, Biolegend, San Diego, CA, USA), human anti-CD14 (PE, Biolegend, San Diego, CA, USA), human anti-HLA-DR (PE, Biolegend, San Diego, CA, USA), human anti-CD33 (PE-Cy7, Biolegend, San Diego, CA, USA), and human anti-CD163 (APC/Cy7, Biolegend, San Diego, CA, USA) for 30 min at 4 °C in the dark. Stained cells were washed by FACS buffer (PBS containing 1% BSA and 0.01% sodium azide) and fixed by 4% paraformaldehyde (Biosesang Inc. Gyeonggi, Korea). Measurement was performed using FACSVerse (BD Biosciences, Franklin Lakes, NJ, USA) and FlowJo software (TreeStar, San Carlos, CA, USA).

2.7. Magnetic cell sorting for CD34 positive cells

Healthy donor blood was collected and removed RBCs using RBC lysis buffer (Biolegend) and washed using MACS buffer (PBS containing 5 mg/ml BSA and 2 mM EDTA). CD34+ cells were isolated using CD34 microbead kit (Miltenyi Biotec, Auburn, CA, USA) according to the manufacturer’s instructions.

2.8. Cytokine array

Serum was collected from human and Hu-PBL-NSG mice. Cytokine

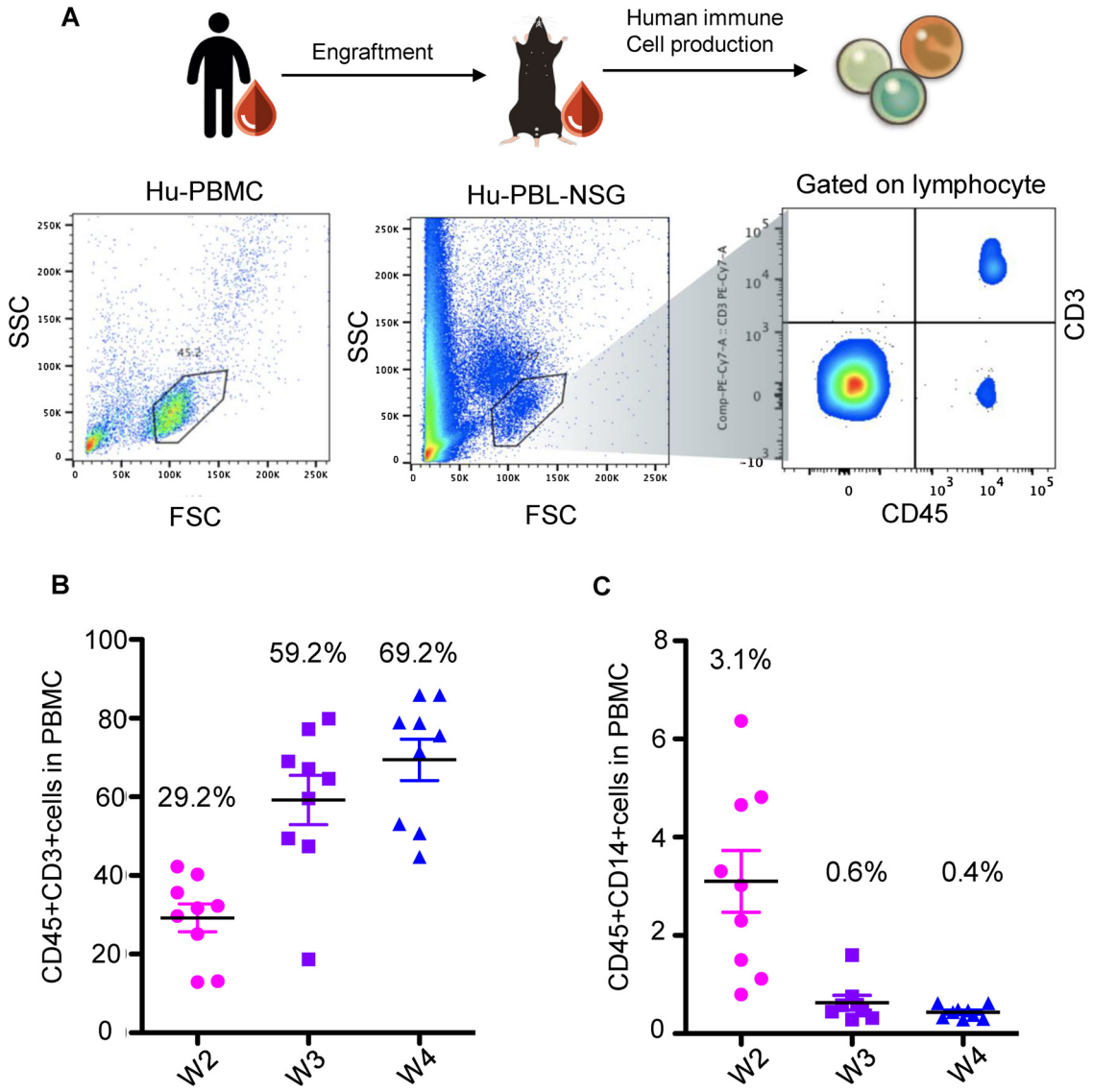

Fig. 1. Immune cell population after engraftment of human PBMCs in NSG mice (A) Gating protocol of $CD3^+CD45^+$ cells (B–C) human T cells and monocytes were measured by surface markers; $CD3^+CD45^+$ and $CD14^+CD45^+$ respectively until week 4 (N = 9).

array profile was analyzed using RayBio C-Series Human Th1/Th2/Th17 antibody array C1 kit (RayBiotech, Norcross, Georgia, USA) following to manufacturer's instructions. Imaging data was analyzed by ImageJ software (US National Institutes of Health, Bethesda, Maryland, USA) for the measurement of cytokine intensity. The intensity spots were logged and then normalized by positive control. The normalized data was re-normalized by quintile normalization module in R (R-Studio, Inc., Boston, MA, USA). The folds and p-value were analyzed by R.

2.9. Histology and immunohistochemistry

Tissues were fixed in 10% neutral-buffered formalin (Fisher Scientific, Orangetown, NY, USA), embedded in paraffin, and sectioned 4 μm. Tissues were stained with hematoxylin and eosin (H&E). Additional sections were stained by immunohistochemistry using anti-CD3 rabbit (Abcam, ab16669, Cambridge, MA, USA) and a streptavidin-HRP system (Dako, Carpinteria, CA, USA).

2.10. Multispectral imaging

Multispectral images (MSI) were produced with the Vectra Polaris system (PerkinElmer, Akron, OH, USA), where at least fifteen MSIs from a tissue sample were obtained. By InForm 2.3.0 software (PerkinElmer, Akron, OH, USA), each fluorophore representative markers were individually separated, which was used for the color-based identification of cell types and levels of marker expression. To quantify and compare cell number and expression target protein in tumor nest and stroma, respective regions were automatically determined by pattern-training manner supported by the InForm software. Sections were incubated with primary antibodies for 30–60 min at room temperature followed by a secondary horseradish peroxidase (HRP)-conjugated polymer (PerkinElmer, Akron, OH, USA) for 10 min at room temperature. A 6-plex quantitative immunohistochemistry (IHC) assay (OPAL, PerkinElmer, Hopkinton, MA, USA) was added to the sections in which the target proteins as well as antibody complexes were coated with fluorescent dyes activated by HRP. After staining, bound antibody complexes and non-reacted fluorescence dyes were removed by additional antigen retrieval step. Whole steps were repeated through seven sequential rounds for multispectral staining. Finally, Spectral DAPI

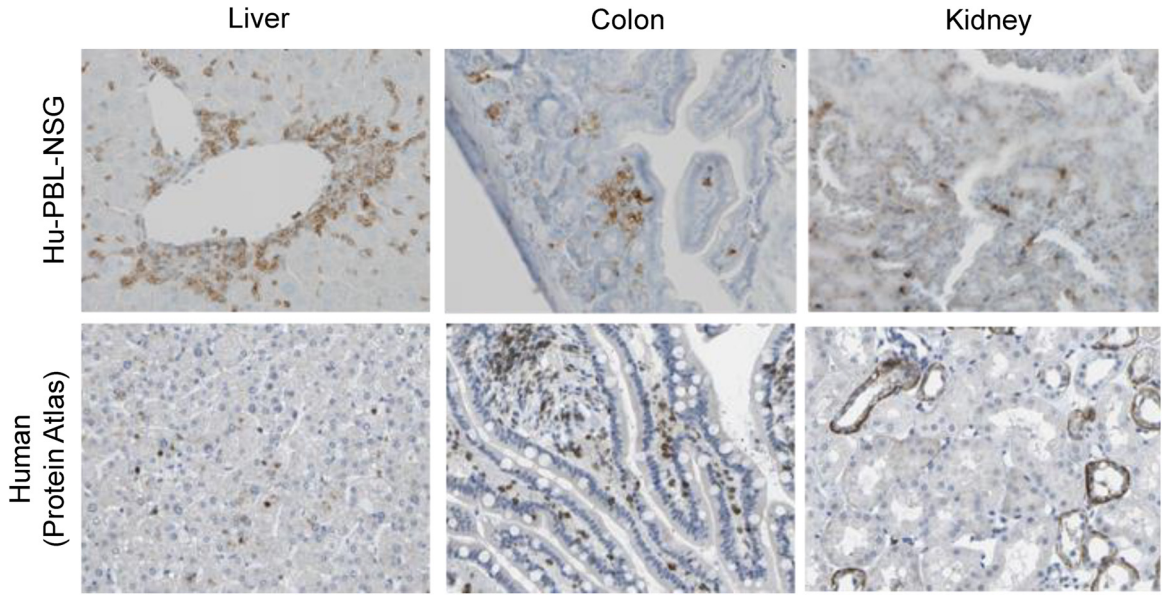

Fig. 2. Histologic analyses of Hu-PBL-NSG mouse model Lung, colon and kidney tissue stained with anti-CD3 antibody in Hu-PBL-NSG mouse (above) compared to human tissue (Referenced from 'The Human Protein Atlas', https://www.proteinatlas.org/ENSG00000198851-CD3E/tissue, below) (4–5 weeks after engraftment, a representative picture among 9 mice).

reagent (PerkinElmer, Akron, OH, USA) was used for counter staining. For image preparation, all stained section was mounted with Antifade Mounting Medium (Vector Labs, Burlingame, CA, USA). For IHC, Bond Poly Refine Detection kit was used according to the programed protocol in Bond RX auto-stain system (Leica, Nussloch, Germany). Antibodies for CD8, CD11b, CD68 and FoxP3 were used for confirmation of infiltrating immune cells originated human PBL. For investigation of tumor microenvironment, antibodies for CD3, CD8, FoxP3, PD-1, PD-L1 and pan-cytokeratin were used.

2.11. Microarray and analysis

Tumor RNA was extracted for microarray HG-U133 plus 2.0 processing and hybridization. The two groups, control (N = 2) and anti-PD-1 treated group (N = 2), were compared by gene set enrichment analysis (GSEA) after normalization with robust multi array average algorithm (RMA). The 'Gene Ontology (GO)' was applied for GSEA analysis.

2.12. Statistical analysis

All data were expressed as the mean ± standard error (SE). Statistical analyses of all data were performed by GraphPad Prism (Version 5, GraphPad Software, Inc). Differences between groups were tested by two-tailed paired Student *t* test and $p < 0.05$ is determined as significant.

3. Results

3.1. Human CD3 dominance in Hu-PBL-NSG mouse model

Circulating human T cells ($hCD3^+hCD45^+$) and monocytes ($hCD45^+$ $hCD14^+$) were measured after 2 week, 3 weeks and 4 weeks by FACS in established Hu-PBL-NSG mice. The gating protocol of $CD3^+CD45^+$ cells were shown in Fig. 1**A**. The proportion of $CD45^+CD3^+$ cells, which represent T cells, showed an increase until week 4 (2-3-4 weeks, 29.2–59.2-69.2% respectively) (Fig. 1B), whereas the proportion of CD45 + CD14 +, which represent monocytes, did not increase (2-3-4 weeks, 3.1-0.6-0.4% respectively, Fig. 1C). M2 macrophage and myeloid derived suppressor cells (MDSCs) were also observed in splenocytes of Hu-PBL-NSG mouse model (Supplementary Fig. 3).

Hu-PBL-NSG mice were then sacrificed and internal organs were collected for investigating $CD3^+$ immune cell infiltration. Lung, liver, colon and kidney tissue were stained with anti-CD3 antibody (Fig. 2), and were compared with those of human in protein atlas. $CD3^+$ T cells were observed in alveoli, liver, lamina propria of colon and renal tubules. Given that NSG mice do not produce lymphocytes, these findings imply that human immune cells have been well established.

3.2. Immune cell distribution in various organs of hu-PBL-NSG model

Multispectral imaging of various organs was analyzed in Hu-PBL-NSG mice with anti- Foxp3, CD8, CD11b antibodies. Regulatory T cells (Treg, [3.6%]), $CD8^+$ T cell (36.09%), and $CD11b^+$ myeloid cells (16.51%) were observed in spleen of Hu-PBL-NSG mouse model (left panel: RAW MSI image, right panel: immune cell phenotyping data) (Fig. 3A). In addition, we observed various organs for the infiltration of immune cells. As expected, lung, colon, kidney and liver were infiltrated with Tregs, $CD8^+$ cells and CD11b + cells (Fig. 3B). The cell population of Treg, $CD8^+$ cells and $CD11b^+$ cells were: 0.30%, 37.25%, 6.58% in lung, 0.22%, 0.16%, 1.40% in colon, 0.04%, 4.24%, 13.69% in kidney, 0%, 7.02%, 1.21% in liver, respectively.

3.3. Serological similarity between human PBMCs and Hu-PBL-NSG mouse model

Next, we compared serological similarity between human PBL and Hu-PBL-NSG mouse model. The serum of donor and Hu-PBL-NSG mouse were extracted and compared by cytokine array. The heatmap shows the expression of various cytokines from donor and Hu-PBL-NSG mouse (Fig. 4A). Individual and functional differences in cytokines are shown in Fig. 4B. Overall, cytokine pattern was similar between human and mouse. Th1-related cytokines such as IFN-gamma and TRANCE, were increased in NSG mice compared to human PBMCs. Among Th2-related cytokines, CD30 and IL-5 were higher, but IL-6sR was lower in Hu-PBL-NSG model. Among tolerance-related cytokines, IL-10 was higher (> 4 folds, $P < 0.05$) in Hu-PBL-NSG model. Interestingly, GM-CSF was dramatically increased (> 40 folds, $P < 0.05$) in Hu-PBL-NSG model. GM-CSF is an important factor of myeloid cell generation in this

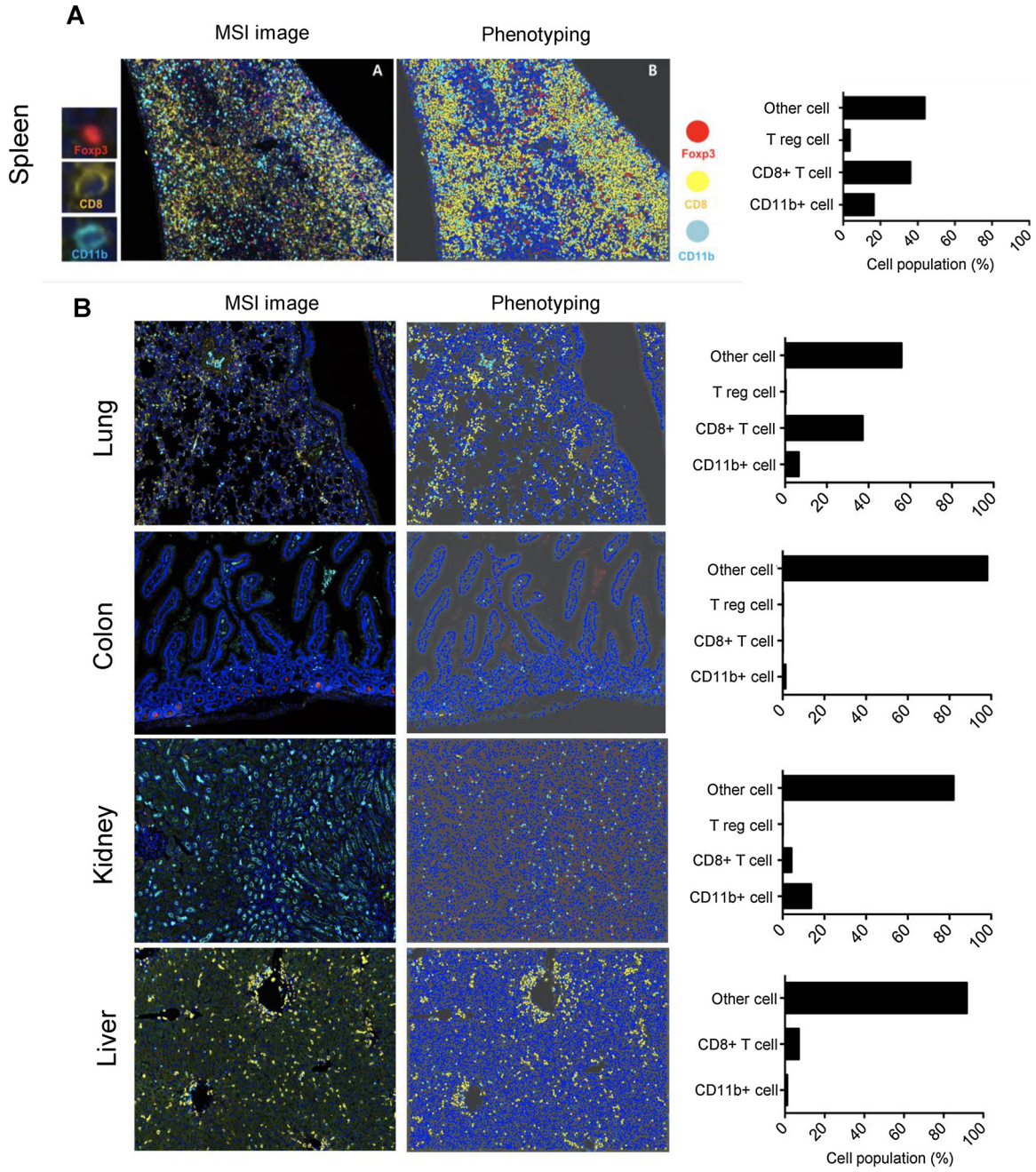

Fig. 3. Multispectral imaging (MSI) of various organs in Hu-PBL-NSG mouse model (A) Raw multispectral and phenotype images of spleen with Foxp3, CD8 and CD11b markers (representative picture, 4–5 weeks after engraftment), (B) Raw multispectral and phenotype images of variable organs with Foxp3, CD8 and CD11b markers (lung, colon, kidney and liver).

model for macrophage, DC, and MDSC differentiation, and could be attributed to abundant T cell population in this model (Fig. 4B).

While Hu-PBL-NSG model was enriched with T lymphocytes, we also observed hCD11c$^+$ cells in spleen, lung, liver and kidney (Fig. 4C). On FACS analysis, the proportion of CD11c$^+$ cells was 20.7% in spleen, 14.7% in lung, 16.8% in liver and 0.51% in kidney. The presence of CD11c$^+$ cells, which represents dendritic cells, suggests that antigen presenting is possible in our model.

We also observed the CD34$^+$ cells in a minority of population (0.09%) from donor's PBMCs (Fig. 4C). Of note, CD34$^+$ cell population increased to 40.8% on FACS *via* MACS concentration. The abundance of CD34$^+$ cells is important for the optimal development of hematopoietic cell lineages in immune avatar models. We assume that the myeloid cell propagation was activated by GM-CSF. As previously seen in the cytokine array, increased GM-CSF expression could enable myeloid cell propagation, represented by the abundance of CD34$^+$ cells.

3.4. Establishment of EML4-ALK cell line and PDX model in Hu-PBL-NSG mice

Two different models were established: 1) allogeneic cell line model consisting of human cancer cell line and PBL from a HLA-class 1 matched donor 2) allogeneic avatar consisting of tissue from the patient and PBL from a HLA-class 1 matched donor. We transplanted an *ALK*-positive cell line, H3122 (*EML4-ALK* variant 1), and a patient-derived tumor from *EML4-ALK*-rearranged (*EML4-ALK* variant 1) NSCLC patient in NSG mice. When the tumor size reached approximately 100 mm^3, we sacrificed the mice to investigate the tumor

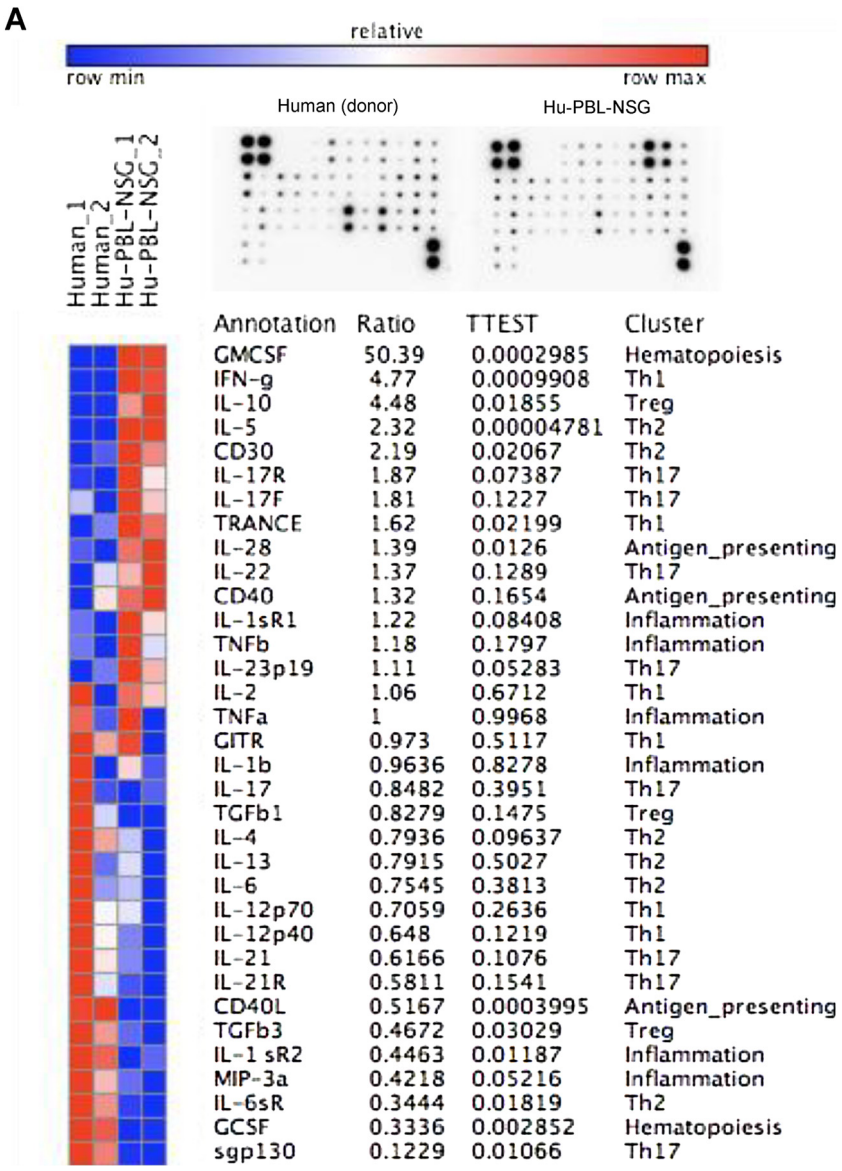

Fig. 4. Serological similarity between human PBMCs and Hu-PBL-NSG mouse model (A) Results of cytokine array for measurement of T cell secretory cytokines. Human serum was used for positive control for comparison between human and Hu-PBL-NSG mouse model. Individual cytokine spots were analyzed log2FC and *p* value (T-TEST). (B) The expression ratio was categorized as Th1, Th2, Th17, immune tolerance, antigen presentation, hematopoiesis, and inflammation (control: n = 3, Hu-PBL-NSG: n = 3, serum of individual group was pooled, repeated twice, and representative picture is shown)., (C) Human-CD11c + cell and CD34+ cell were observed in various tissue and blood respectively. CD34+ cell was clearly observed after MACS sorting (4–5 weeks after engraftment, a representative picture among 3 mice).

microenvironment within the tumors. Multispectral imaging of Hu-PBL-NSG tumors revealed staining of Pan-CK$^+$, PD-L1$^+$, CD3$^+$ T cells, CD8$^+$ T cells, and Foxp3$^+$ cells (Fig. 5A). Tissue was further segmented into tumor (green) and stroma (dark red) and different cells were characterized accordingly. Phenotypic analysis also revealed the presence of CD4+, CD8 + T cells, and Tregs within the tumor. Fig. 5B represents the quantification of multispectral imaging of two models and cells were analyzes by the following markers: cancer, pan-CK$^+$ cell; CD4 cells, CD3$^+$CD8$^-$ cells; CD8 cells, CD3$^+$CD8$^+$ cells; Treg, CD3$^+$Foxp3$^+$ cells. The cell line model had higher CD4 (0.84%), CD8 T cell (2.02%) population in tumor nest, and the population of Treg was lower in the tumor nest compared to stroma (0.1% *vs.* 1.51%). On the contrast, the PDX model had more abundant T cells in the stroma (CD4 T cell: 0.83%, CD8 T cell: 2.02%) compared to the tumor nest (CD4 T cell: 0.29%, CD8 T cell: 0.02%).

3.5. Efficacy of human anti-PD-1 Ab in EML4-ALK cell line model

Next, human anti-PD-1 Ab was treated i.p. (10 mg/kg, twice a week) in H3122 cell line model. Tumor size was measured daily, and after 1 week, the tumor size was significantly smaller compared to vehicle groups in anti-PD-1 Ab-treated model after day 6 (Fig. 6A). Then, tumor was collected from sacrificed mice from both vehicle and anti-PD-1 group, and mRNA was extracted for microarray. On microarray, anti-PD-1 treated group showed increased expression of variable immune response-related genes (Fig. 6B). The top 50 data showed high expression of immune-related genes such as granzyme B, IFN-gamma, LAG-3, CD8a, IL12RB. GSEA revealed increased expression of genes related to immune responses and immune system were observed in anti-PD-1 Ab treated group (Fig. 6C).

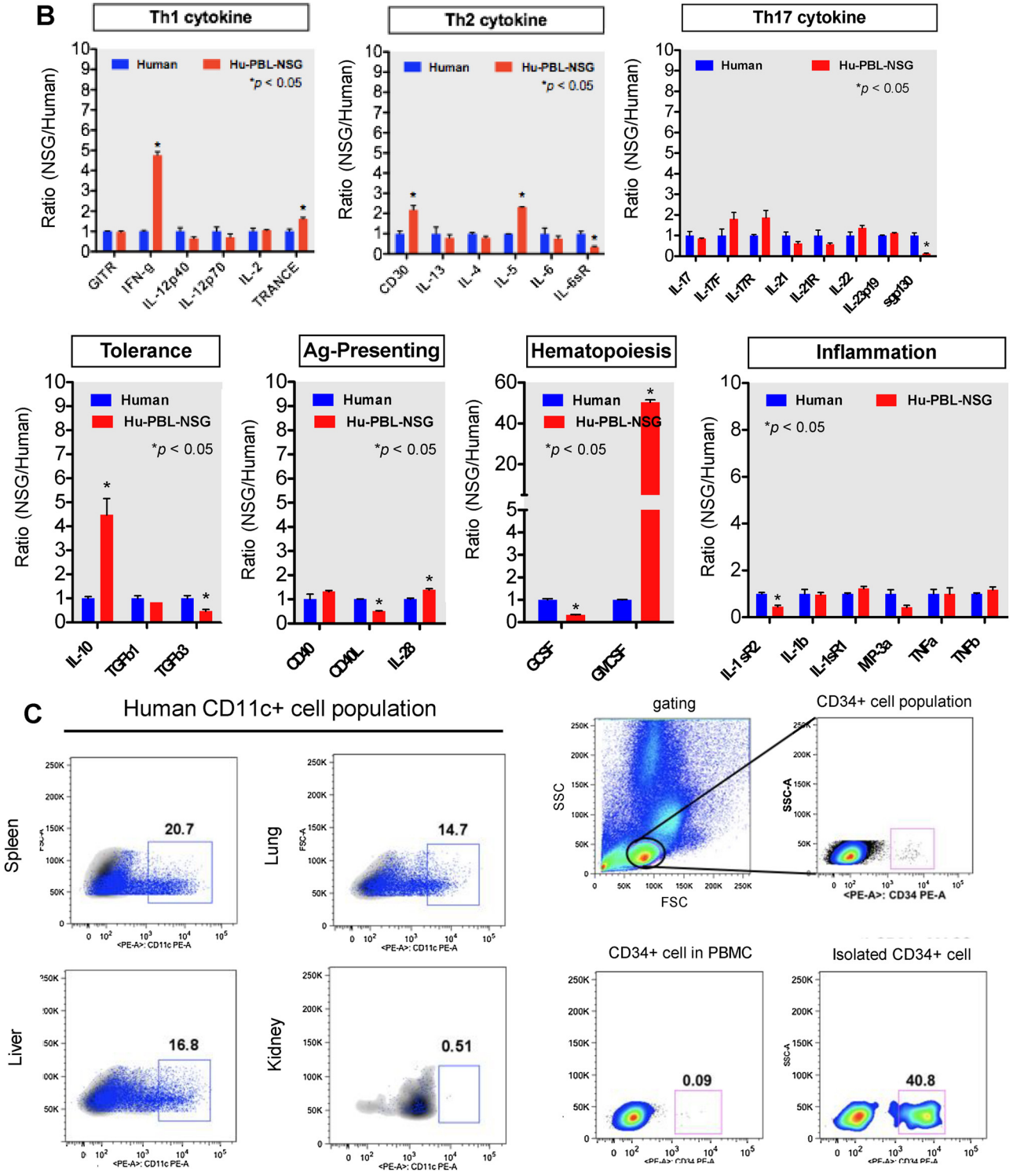

Fig. 4. (*continued*)

4. Discussion

In our study, we successfully established the Hu-PBL-NSG model engrafted with *EML4-ALK* cell line and a patient-derived tumor. Most immune cells were constituted of T cells, but macrophages, dendritic cells and MDSCs were also observed. The major sources of immune cell differentiation, which were $CD34^+$ hematopoietic stem cells and GM-CSF, were identified in our model. This suggests that $CD34^+$ progenitor cells can differentiate into myeloid and lymphoid cells in the peripheral blood of mice. GM-CSF can recruit immature cells to differentiate and mature into effector T cells, activated macrophages, and dendritic cells, all of which constitute tumor immune microenvironment in humans. Immunohistochemical analysis in our study revealed an increase in $CD8^+$ T-cell infiltration of tumor in Hu-PBL-NSG engrafted with H3122 cells. The presence of $CD8^+$ T-cells in tumor is the prerequisite for the antitumor immune response, and may explain the tumor shrinkage in this model.

However, the proportion of tumor infiltrating lymphocytes in the tumor nest and stroma was relatively small (0.1 ~ 2.0%) on multi-spectral imaging, which was concordant with previous study describing

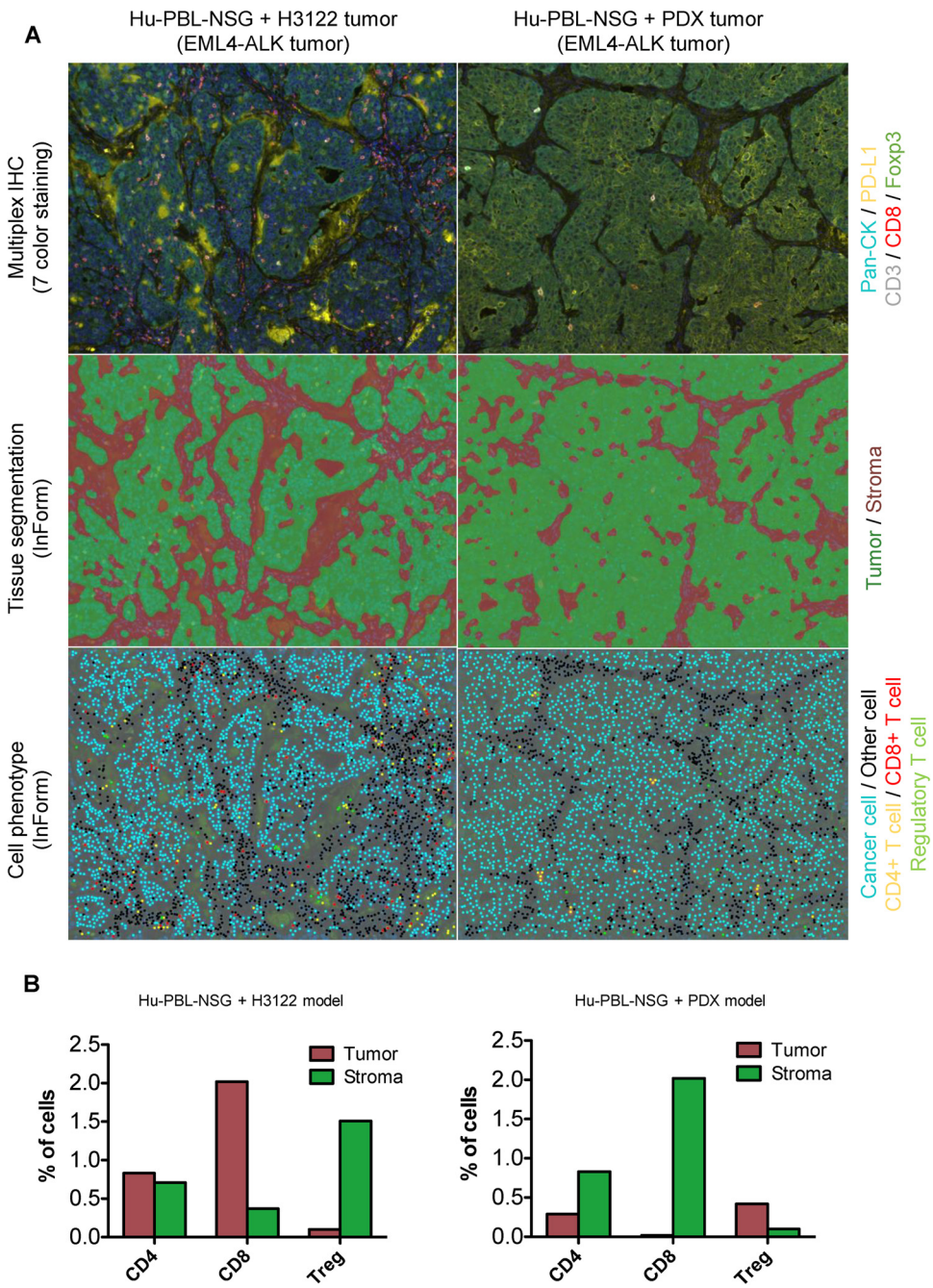

Fig. 5. Multispectral imaging (MSI) of Hu-PBL-NSG tumors. Left is Hu-PBL-NSG mouse with H3122-derived tumor and right is Hu-PBL-NSG mouse with an *ALK* positive patient's tumor xenograft. (A) Top image: RAW image of MSI (5 colored image, cyan: Pan-CK, yellow: PD-L1, white: CD3, red: CD8, and light green: FOXP3), Middle image: tissue segmentation data (green: tumor nest, dark red: stroma region), below image: cell phenotypes (cyan: cancer cell, yellow: CD4 + T cell, red: CD8 + T cell, light green: regulatory T cell). (B) Quantification of immune cells in tumor nest and stroma (For interpretation of the references to colour in this figure legend, the reader is referred to the web version of this article).

that *ALK*-positive tumor has an immune-desert environment [11]. We noted different distribution of tumor infiltrating lymphocytes in the tumor nest and stroma, and this may be due to the difference between tumor cell line *versus* PDX. The PDX tumor engrafted in Hu-PBL-NSG model highly represents human cancers, whereas tumor cell line does not. Tumor cell line has been adapted to grow in two-dimensional cultivation system, in which immune evasion mechanism may not be fully exploited. Consequently, this may contribute to enhanced efficacy to anti-PD-1 therapy in Hu-PBL-NSG model.

Research on cancer immunology has been hindered by the lack of optimal animal models, given that the immune responses of human and non-human species show significant differences. Due to the high cost of clinical trials, it is urgent to improve the current animal models that can mimic faithfully human physiology, particularly the human immune system. We have generated humanized mice by engrafting human PBMCs into highly immuno-deficient mice. This approach has been previously well described by Shultz et al. [12], in which rapid analysis of human immune function was feasible within 4 weeks. The major drawback of allogenic PBMC transplantation is the GVHD response that results in lethality [13,14]. Similarly, although we assessed the early efficacy of anti-PD-1 antibody by tumor shrinkage, our experiments were limited to a time period of 4 weeks post-transplantation due to the issue of GVHD onset. Thus, the therapeutic observational window is restricted to a few weeks before evident signs of GVHD. Recently, a novel major histocompatibility class I- and class II-deficient NOD/Shi-*scid*-IL2rγ^{null} (NOG) mouse model was recently developed which exhibited no signs of GVHD and survived up to 12 weeks [15]. Moreover, injection of human CD34$^+$ hematopoietic stem cells into irradiated host mice is another approach to humanization, which delay the onset of GVHD [7]. Compared to Hu-CD34$^+$ model, Hu-PBL model has several advantages and limitations. Hu-PBL model is simple and economic, and has been widely used in the study of infectious diseases and

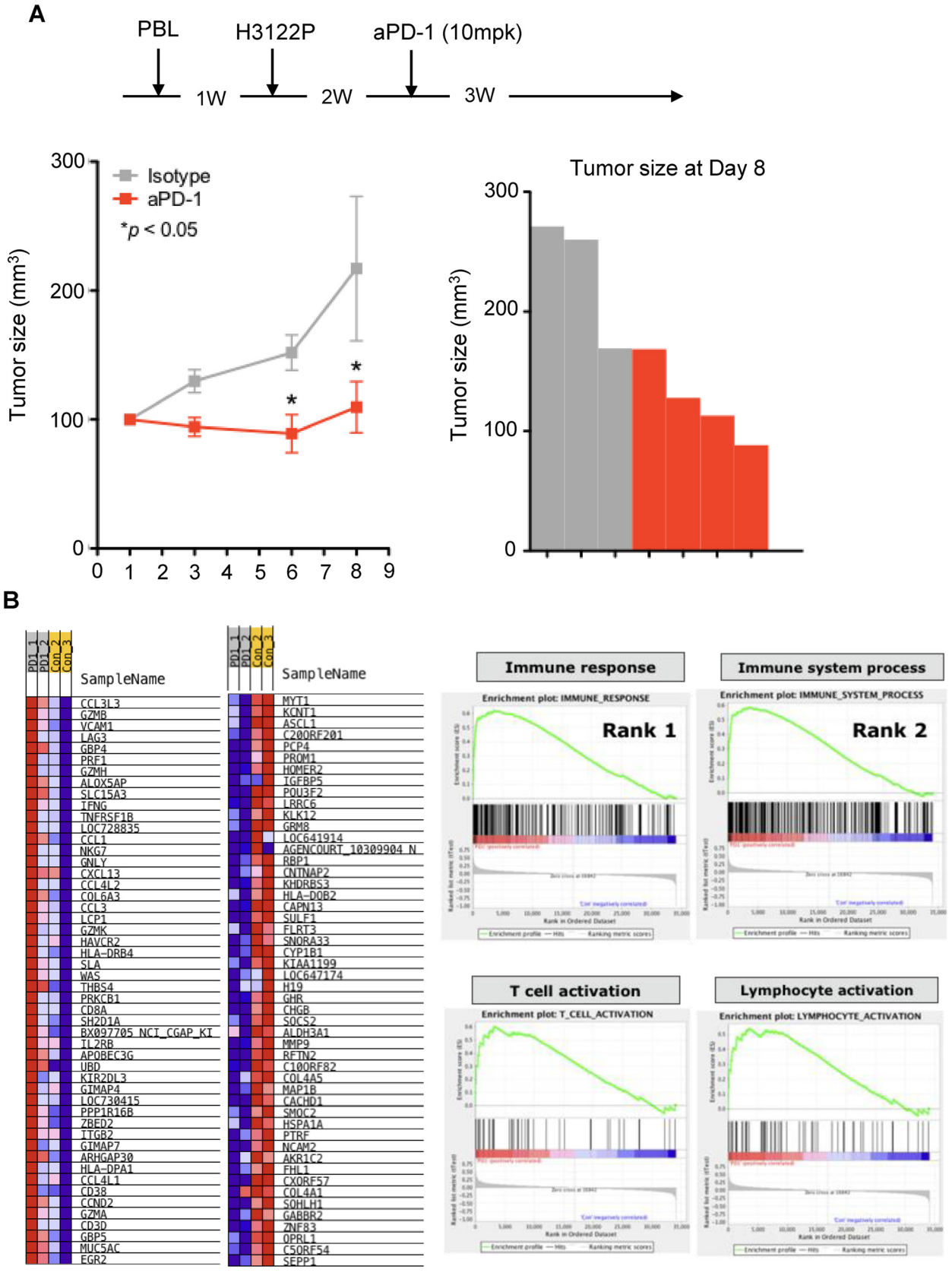

Fig. 6. Anti-tumor effects of anti-PD-1 Ab in H3122 engrafted Hu-PBL-NSG mice. (A) Treatment strategy of anti-PD-1 Ab resulted in significant tumor shrinkage in anti-PD-1 Ab treated mice (10 mpk, Q2W, i.p. injection). (B) Microarray analysis and gene set enrichment analysis of tumor mRNA obtained from vehicle and anti-PD-1 Ab treated mice.

autoimmunity. It takes shorter time for immune reconstitution. Additionally, Hu-PBL model has mature human leukocytes T cells which are active in phenotype, whereas Hu-CD34$^+$ model has different degrees of T cells and monocytes maturation [7].

The utilization of the humanized Hu-PBL-NSG model for *in vivo* drug testing will facilitate the study of immuno-oncology drugs, such as evaluating efficacy of immune checkpoint inhibitors and developing predictive biomarkers [16]. Additionally, these models may recapitulate some adverse autoimmune reactions to immune checkpoint inhibitors [17], which may give insights into mechanisms of immune-related adverse events.

In conclusion, our Hu-PBL-NSG mice recapitulate human cells of the innate and adaptive immune system. Understanding the caveat of humanized mice and developing improved models to delay development of GVHD will facilitate preclinical evaluation of immuno-oncology drugs and heighten translational power.

Conflict of interests

All authors declare no conflicts of interest.

Acknowledgements

SML is supported by the National Research Foundation grant by the Korea government (No. 2016R1C1B1013299), and the Bio & Medical Technology Development Program of the National Research Foundation funded by the Korean government (No. 2018M3A9E8066245). BCC is supported by a Dongin Sports research grant of Yonsei University College of Medicine (6-2017-0104, 6-2018-0115).

Appendix A. Supplementary data

Supplementary material related to this article can be found, in the online version, at doi:https://doi.org/10.1016/j.lungcan.2018.11.035.

References

[1] A. Hoos, Development of immuno-oncology drugs - from CTLA4 to PD1 to the next generations, Nat. Rev. Drug Discov. 15 (2016) 235–247.
[2] M. Reck, D. Rodriguez-Abreu, A.G. Robinson, R. Hui, T. Csoszi, A. Fulop, M. Gottfried, N. Peled, A. Tafreshi, S. Cuffe, M. O'Brien, S. Rao, K. Hotta, M.A. Leiby, G.M. Lubiniecki, Y. Shentu, R. Rangwala, J.R. Brahmer, K.-Investigators, Pembrolizumab versus chemotherapy for PD-L1-Positive non-small-Cell lung Cancer, N. Engl. J. Med. 375 (2016) 1823–1833.
[3] P.C. Tumeh, C.L. Harview, J.H. Yearley, I.P. Shintaku, E.J. Taylor, L. Robert, B. Chmielowski, M. Spasic, G. Henry, V. Ciobanu, A.N. West, M. Carmona, C. Kivork, E. Seja, G. Cherry, A.J. Gutierrez, T.R. Grogan, C. Mateus, G. Tomasic, J.A. Glaspy, R.O. Emerson, H. Robins, R.H. Pierce, D.A. Elashoff, C. Robert, A. Ribas, PD-1 blockade induces responses by inhibiting adaptive immune resistance, Nature 515 (2014) 568–571.
[4] K.R. Voong, J. Feliciano, D. Becker, B. Levy, Beyond PD-L1 testing-emerging biomarkers for immunotherapy in non-small cell lung cancer, Ann. Transl. Med. 5 (2017) 376.
[5] J. Tang, A. Shalabi, V.M. Hubbard-Lucey, Comprehensive analysis of the clinical immuno-oncology landscape, Ann. Oncol. 29 (2018) 84–91.
[6] L.D. Shultz, M.A. Brehm, J.V. Garcia-Martinez, D.L. Greiner, Humanized mice for immune system investigation: progress, promise and challenges, Nat. Rev. Immunol. 12 (2012) 786–798.
[7] P. De La Rochere, S. Guil-Luna, D. Decaudin, G. Azar, S.S. Sidhu, E. Piaggio, Humanized mice for the study of immuno-oncology, Trends Immunol. 39 (2018) 748–763.
[8] M.F. Sanmamed, C. Chester, I. Melero, H. Kohrt, Defining the optimal murine models to investigate immune checkpoint blockers and their combination with other immunotherapies, Ann. Oncol. 27 (2016) 1190–1198.
[9] D.E. Mosier, R.J. Gulizia, S.M. Baird, D.B. Wilson, Transfer of a functional human immune system to mice with severe combined immunodeficiency, Nature 335 (1988) 256–259.
[10] M.A. Brehm, M.V. Wiles, D.L. Greiner, L.D. Shultz, Generation of improved humanized mouse models for human infectious diseases, J. Immunol. Methods 410 (2014) 3–17.
[11] J.F. Gainor, A.T. Shaw, L.V. Sequist, X. Fu, C.G. Azzoli, Z. Piotrowska, T.G. Huynh, L. Zhao, L. Fulton, K.R. Schultz, E. Howe, A.F. Farago, R.J. Sullivan, J.R. Stone, S. Digumarthy, T. Moran, A.N. Hata, Y. Yagi, B.Y. Yeap, J.A. Engelman, M. Mino-Kenudson, EGFR mutations and ALK rearrangements are associated with low response rates to PD-1 pathway blockade in non-small cell lung Cancer: a retrospective analysis, Clin. Cancer Res. 22 (2016) 4585–4593.
[12] T. Pearson, D.L. Greiner, L.D. Shultz, Creation of "humanized" mice to study human immunity, Curr. Protoc. Immunol. 15 (2008) 21 Chapter 15: Unit.
[13] M. Ito, H. Hiramatsu, K. Kobayashi, K. Suzue, M. Kawahata, K. Hioki, Y. Ueyama, Y. Koyanagi, K. Sugamura, K. Tsuji, T. Heike, T. Nakahata, NOD/SCID/gamma(c) (null) mouse: an excellent recipient mouse model for engraftment of human cells, Blood 100 (2002) 3175–3182.
[14] M.A. King, L. Covassin, M.A. Brehm, W. Racki, T. Pearson, J. Leif, J. Laning, W. Fodor, O. Foreman, L. Burzenski, T.H. Chase, B. Gott, A.A. Rossini, R. Bortell, L.D. Shultz, D.L. Greiner, Human peripheral blood leucocyte non-obese diabetic-severe combined immunodeficiency interleukin-2 receptor gamma chain gene mouse model of xenogeneic graft-versus-host-like disease and the role of host major histocompatibility complex, Clin. Exp. Immunol. 157 (2009) 104–118.
[15] T. Ashizawa, A. Iizuka, C. Nonomura, R. Kondou, C. Maeda, H. Miyata, T. Sugino, K. Mitsuya, N. Hayashi, Y. Nakasu, K. Maruyama, K. Yamaguchi, I. Katano, M. Ito, Y. Akiyama, Antitumor effect of programmed Death-1 (PD-1) blockade in humanized the NOG-MHC double knockout mouse, Clin. Cancer Res. 23 (2017) 149–158.
[16] M. Wang, L.C. Yao, M. Cheng, D. Cai, J. Martinek, C.X. Pan, W. Shi, A.H. Ma, R.W. De Vere White, S. Airhart, E.T. Liu, J. Banchereau, M.A. Brehm, D.L. Greiner, L.D. Shultz, K. Palucka, J.G. Keck, Humanized mice in studying efficacy and mechanisms of PD-1-targeted cancer immunotherapy, FASEB J. 32 (2018) 1537–1549.
[17] N.K. Vudattu, F. Waldron-Lynch, L.A. Truman, S. Deng, P. Preston-Hurlburt, R. Torres, M.T. Raycroft, M.J. Mamula, K.C. Herold, Humanized mice as a model for aberrant responses in human T cell immunotherapy, J. Immunol. 193 (2014) 587–596.